Measurement of Neutral and Charged Current Cross Sections at High Q^2

Manfred Fleischer
for the H1 Collaboration at HERA

Institut für Physik, Universität Dortmund, D-44221 Dortmund, Germany
E-mail: manfred.fleischer@desy.de

A preliminary cross section measurement for neutral and charged current processes in deep inelastic e^+p scattering is reported for a range in Q^2 from 200 to 30000 GeV^2. The data were collected by the HERA H1 experiment during the years 1994 – 1997, corresponding to an integrated luminosity of 37 pb^{-1}. The data are used to compare with electroweak predictions and to test QCD evolutions at high Q^2 and large x-Bjorken values up to 0.65.

1 Introduction

At HERA deep inelastic scattering (DIS) can be studied in kinematic domains beyond those of fixed target experiments due to the high center of mass energy of about 300 GeV of head on collisions with 27.6 GeV positrons on 820 GeV protons.

In the first years of HERA operation (92–94) the domain of low momentum transfer squared Q^2 and small Bjorken-x has been extensively studied [1]. Most recent high precision H1 results on low Q^2 NC interactions are described elsewhere [2].

With a tenfold increase of statistics, compared to the first years, the domain of high Q^2 is being explored with significantly improved statistical and systematic precision. In this contribution recent results on high Q^2 data are briefly discussed. Further details of the analysis can be found in [3]. For both neutral current (NC) and charged current (CC) interactions single and double differential cross sections are measured, probing directly the valence quark region at high x. The measured cross sections and the extracted structure function F_2 as well as the determined W propagator mass M_W are discussed in the framework of the Standard Model.

2 Experimental Techniques

2.1 Reconstruction of Kinematic Variables

The measurement of differential cross sections in DIS relies crucially on the precise determination of kinematic variables. In case of neutral current interactions both the scattered positron and the hadronic final state are measured, allowing several complementary approaches for the determination of kinematic variables. In the case of charged currents the final state neutrino escapes detection, such that only the hadronic final state can be used. By introducing the sum over all particles of the hadronic final state Σ and the transverse momentum $P_{T,h}$:

$$\Sigma = \Sigma_h(E_h - p_z) \quad , \quad P_{T,h} = \sqrt{(\sum_h p_{x,h})^2 + (\sum_h p_{y,h})^2}$$

the kinematic variables according to [4] are:

$$y_h = \frac{\Sigma}{2\ E_e} \ , \ Q_h^2 = \frac{P_{T,h}^2}{1-y_h} \ , \ x_h = \frac{Q_h^2}{s\ y_h}$$

Q_h^2, x_h and y_h have to be used in case of CC interactions. In NC measurements a combined approach using both, hadron and positron quantities is applied:

$$Q_{e\Sigma}^2 = \frac{E_e'^2 \sin^2\theta_e}{1-y_e} \ , x_{e\Sigma} = \frac{E_e'^2 \sin^2\theta_e}{s\ y_\Sigma(1-y_\Sigma)} \ \text{with}\ y_\Sigma = \frac{\Sigma}{E-p_z}$$

Using this so-called $e\Sigma$ method [5] the best resolution in the complete kinematic range is achieved for H1.

2.2 The H1 Detector

The H1 detector [6] was built as a multi-purpose apparatus with almost 4π coverage. In the measurement of interactions at high Q^2 the tracking system and the Liquid Argon (LAr) Calorimeter [7] are primarily involved. Both, the tracking system and the LAr calorimeter are surrounded by a superconducting magnet, which provides a magnetic field of 1.15 T.

Tracks in the central H1 detector are measured in two concentric drift chambers with a transverse momentum resolution of $\delta P_T/P_T < 0.01 P_T/\text{GeV}$. Both forward and central tracking chambers are used for the determination of the z-vertex position.

At high Q^2 the hadronic final state, as well as the scattered positron in case of NC events, are detected in the highly segmented LAr calorimeter, consisting of about 44000 cells. The stable performance of the LAr calorimeter [8] as well as intensive work on alignment and in situ calibration lead to a good knowledge of the electromagnetic energy scale to better than 1% in the medium Q^2 range ($100 < Q^2 < 1000$ GeV^2) and better than 3% at higher Q^2. The hadronic energy scale is known with an uncertainty between 3 and 4%.

The luminosity measurement is based on the detection of Bethe-Heitler events $ep \rightarrow ep\gamma$, where two calorimeters close to the beampipe are employed [9]. For the presented measurement the precision of the integrated luminosity determination is 2.6% [10].

In order to trigger high Q^2 events a system of projective trigger towers is used, where the response in neighbouring calorimeter cells are combined and summed. These towers, pointing to the vertex region, have a trigger efficiency of 99.5% for electromagnetic cluster energies above 11 GeV. In case of CC events the missing transverse momentum P_T^{miss} is constructed on the basis of trigger towers. Here an efficiency of $(50 \pm 5)\%$ is reached for a P_T^{miss} above 12 GeV rising to $(95 \pm 0.5)\%$ above 25 GeV.

2.3 Selection and Simulation

The high Q^2 analysis is based on data of positron proton collisions recorded between 1994 and 1997, corresponding to an integrated luminosity of 37.0 pb^{-1}. The selection of NC events is based on the identification of the scattered positron within the acceptance of the LAr calorimeter, complemented by a set of fiducial cuts. In CC events the neutrino is tagged by the transverse momentum P_T of the hadronic final state. In total about 75000 NC events and about 700 CC events were selected and accepted after applying some background filters against beam-gas events and cosmic particle interactions.

The H1-detector response is simulated using the GEANT package [11]. Using similar Monte Carlo techniques, the acceptance corrections and background contributions are determined. DIS processes are generated using the DJANGO generator [12], which is employing HERACLES [13] for the electroweak interaction. ARIADNE [14] and LEPTO [15] are used for the hadronisation. After generation and detector simulation the high statistics Monte Carlo event samples are computed using the same reconstruction and analysis chain as for real ep data. The Monte Carlo events generated with the MRSH parton distribution [16] are reweighted according to the H1 QCD fit in case of NC. For the CC sample no reweighting is performed.

3 Cross Section Measurements

All cross sections discussed in the following are corrected for QED radiation effects. The radiative corrections are determined using HERACLES [13] in case of NC and HECTOR [17] in case of CC cross sections.

3.1 NC Cross Sections at High Q^2

The cross sections for $e^+p \to e^+X$ in the case of unpolarized beams is:

$$\frac{\mathrm{d}^2\sigma}{\mathrm{d}x\,\mathrm{d}Q^2} = \frac{2\pi\alpha^2}{xQ^4}\left[Y_+F_2(x,Q^2) - y^2F_L(x,Q^2) - Y_-\,xF_3(x,Q^2)\right]$$

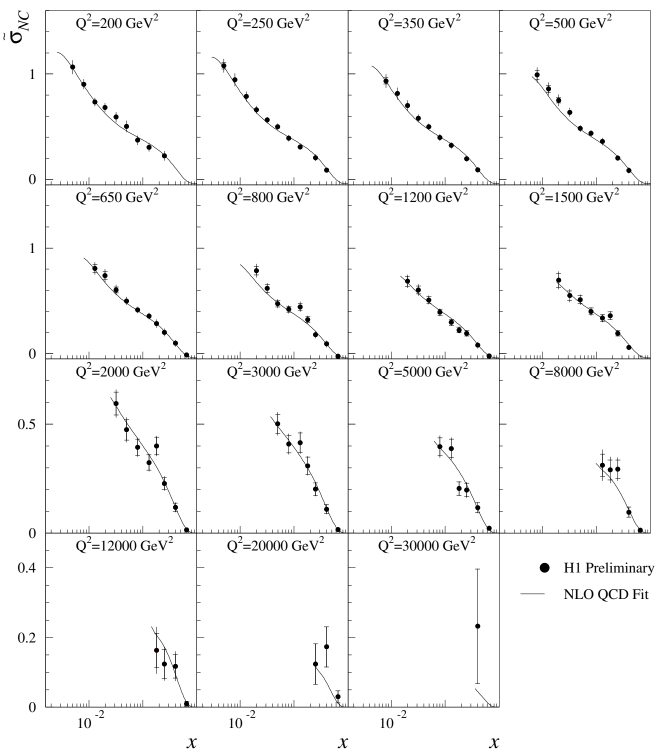

Figure 1: The reduced NC cross section as function of x, compared with the NLO QCD fit, for different values of Q^2.

where the helicity dependence of electroweak interactions is contained in the functions $Y_\pm(y) = 1 \pm (1-y)^2$. Here F_2, F_L and xF_3 are generalized proton structure functions. In the kinematic domain of 200 $\mathrm{GeV}^2 \leq \mathrm{Q}^2 \leq$ 30000 GeV^2 and $0.005 \leq x \leq 0.65$ the structure function F_2 can be decomposed as

$$\begin{aligned} F_2 &= F_{em} + \frac{Q^2}{(Q^2+M_Z^2)}F_{int} + \frac{Q^4}{(Q^2+M_Z^2)^2}F_{wk} \\ &= F_{em}(1+\delta_Z) \end{aligned}$$

where F_{em} considers the photon exchange, F_{wk} the Z° exchange and F_{int} the γZ° interference.

The contributions from Z exchange and γZ interference are important only for $Q^2 > 1500$ GeV^2. The contribution of F_L is calculated to be small in the high Q^2 region, below 5% at highest y values and negligible at lower y.

The cross sections are presented in the next paragraphs in the form of so-called reduced cross sections. This diminishes the influence of the propagators and resembles F_2 at low Q^2 and y:

$$\tilde{\sigma}(e^+p) \equiv \frac{xQ^4}{2\pi\alpha^2}\frac{1}{Y_+}\frac{\mathrm{d}^2\sigma}{\mathrm{d}x\mathrm{d}Q^2}$$

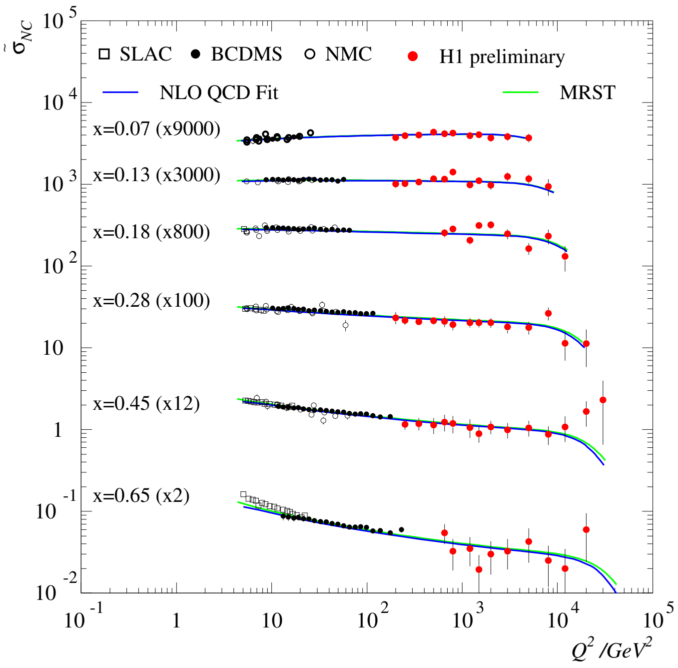

Figure 2: The reduced NC cross section at high x, compared to the MRST parton density function and the NLO QCD fit.

3.2 Double Differential Cross Sections in NC

In Fig. 1 the reduced double differential cross section is shown as a function of x for Q^2 values between 200 and 30000 GeV^2. The rise of $\tilde{\sigma}$ at low x reflects the increase of the sea quark and gluon densities. The NLO order fit[3], based on the DGLAP equations[18], applied to these data gives a good description of the measured cross sections. While at high Q^2 beyond 1000 GeV^2 the accuracy of the measurements is dominated by statistical errors, the measurements below 1000 GeV^2 are dominated by systematic effects, such as the electromagnetic and hadronic energy scale uncertainties.

In order to investigate the region of high x, where an excess of data over Standard Model prediction was reported[19], the reduced cross section is shown in Fig. 2 for values of x between 0.07 and 0.65 as function of Q^2. At x =0.45 an excess is visible, but with decreased significance after inclusion of 1997 data. The measured cross section is here compared to the MRST parton density function[20] and to the NLO QCD fit, which is up to 5% lower than MRST in the high x domain, influenced by the high Q^2 data.

3.3 Sensitivity to γZ Interference

In the region of very high Q^2 the NC cross section is expected to become sensitive to the γZ interference. This is shown in Fig. 3 for two subsamples via the differential cross section dσ/dx. In the upper plot of Fig. 3 events

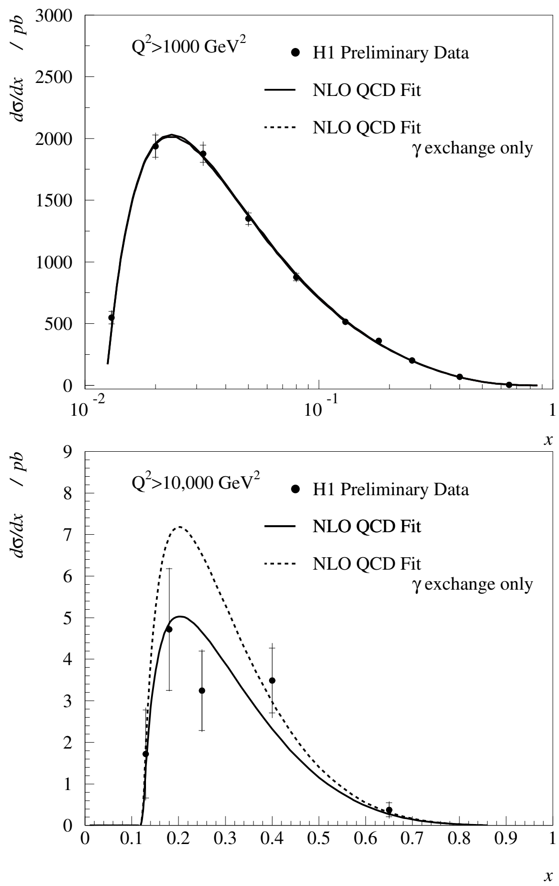

Figure 3: The NC cross section $d\sigma/dx$ at high Q^2, compared with the Standard Model prediction and with the prediction if the coupling to the Z boson is not taken into account.

with a Q^2 larger than 1000 GeV^2 have entered. The data are well described assuming pure γ exchange. In the lower plot, where NC events with a Q^2 larger than 10000 GeV^2 were considered, the two predictions are significantly different, depending on whether or not the γZ interference terms are taken into account. The data agree with the Standard Model prediction and disfavour at a level of 3 standard deviations the assumption of only γ exchange.

3.4 Structure Function Results

In Fig. 4 the preliminary results on the structure function F_2 are shown for the high Q^2 data sample comprising the data 1994-1997. In the low Q^2 domain the published F_2 values are displayed. A wide area of the kinematic plane has been explored by H1. The H1 QCD fit, based on the DGLAP equations in NLO, describes the data well, although that fit was performed only on the low Q^2 data sample[21]. The scaling violation, predicted by perturbative QCD, is clearly visible in the slope as a function of Q^2 for different values of x.

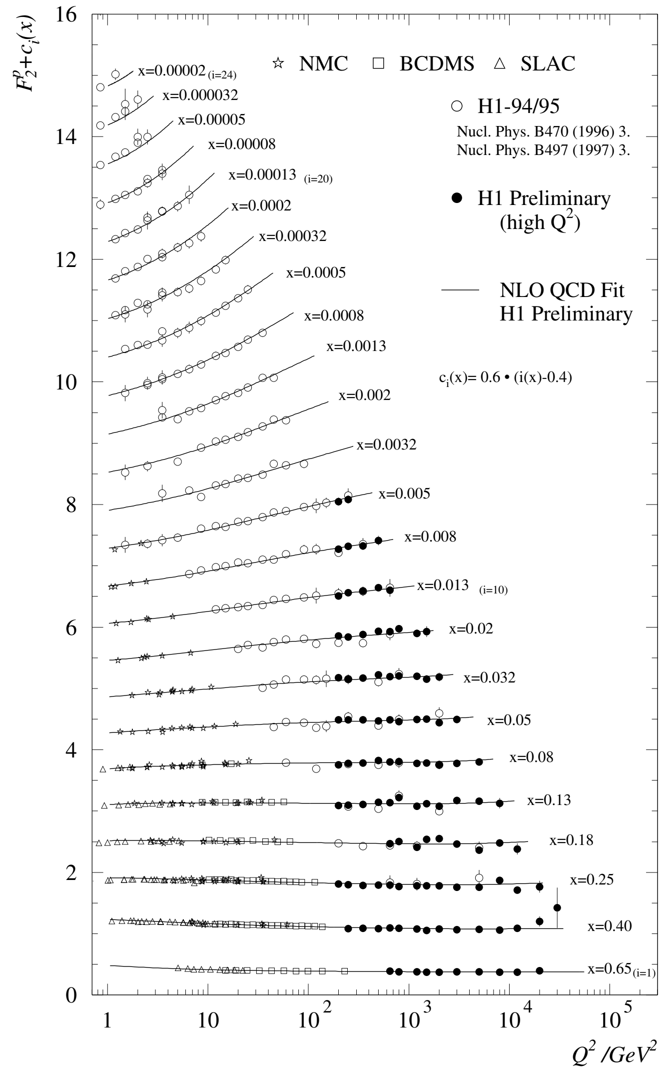

Figure 4: F_2^p ($\equiv F_2^{em}$) results for Q^2 between 1 GeV^2 and 30000 GeV^2 and x between 0.00002 and 0.65 by assuming xF_3 and F_L according to the Standard Model. The NLO fit on the low Q^2 data, based on DGLAP equations, describes all data well.

3.5 CC Cross Sections at High Q^2

Neglecting the effect of quark mixing, the cross section for $e^+p \longrightarrow \bar{\nu}X$ is related to the quark parton densities (xu, xd, xs, xc), which are functions of x and Q^2:

$$\frac{\mathrm{d}^2\sigma}{\mathrm{d}x\mathrm{d}Q^2} = \frac{G_F^2}{2\pi}\frac{M_W^4}{(M_W^2+Q^2)^2}\left[\bar{u}+\bar{c}+(1-y)^2(d+s)\right]$$

In analogy to the NC case the reduced cross section can be defined as:

$$\tilde{\sigma}_{CC} \equiv x\cdot\frac{2\pi}{G_F^2}\frac{(M_W^2+Q^2)^2}{M_W^4}\frac{\mathrm{d}^2\sigma}{\mathrm{d}x\mathrm{d}Q^2}$$
$$= x\cdot\left[\bar{u}+\bar{c}+(1-y)^2(d+s)\right]$$

Note that the y dependence can not be factored out.

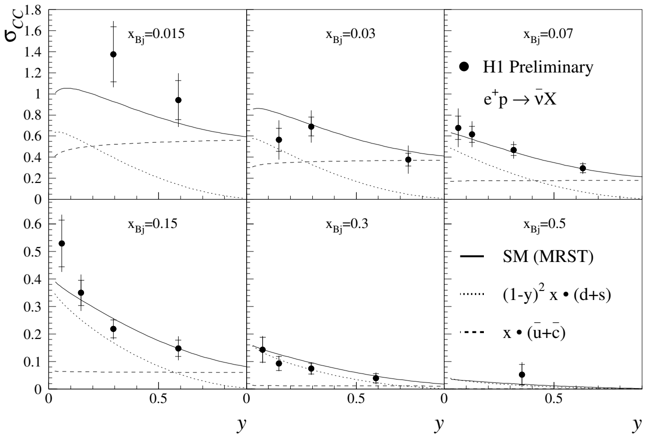

Figure 5: The reduced CC double differential cross section as function of y for different x, compared to the Standard Model prediction using the MRST parton density function. The contributions of valence quarks (d, s) and sea antiquarks $(\bar{u}, \bar{c})$ are shown in dotted/dashed graphs.

3.6 Double Differential Cross Sections in CC

The CC double differential cross section is measured for the first time at high Q^2. In Fig. 5 the result is shown in its reduced form for different bins in x as function of y. The errors at high Q^2 are dominated by the statistical error and the uncertainty of the hadronic energy scale. Within the errors good agreement to the Standard Model prediction can be seen.

In the high x region the cross section is dominated by the term $(1-y)^2(xd)$, which describes the valence quark contribution. At smaller x the sea quark contribution becomes more important.

3.7 Comparison of NC and CC Cross Sections

According to the Quark Parton Model, different quark flavours are involved in the DIS process:

$$NC: \quad \tilde{\sigma}_{NC} \sim x\cdot\left[\frac{4}{9}(u+\bar{u}+c+\bar{c})+\frac{1}{9}(d+\bar{d}+s+\bar{s})\right]$$
$$CC: \quad \tilde{\sigma}_{CC} \sim x\cdot\left[\bar{u}+\bar{c}+(1-y)^2(d+s)\right]$$

At high x the contributions of sea quarks can be neglected, and thus a direct comparison of u-quark density (NC) and d-quark density (CC) can be obtained by the comparison of the structure function terms $Y_+\,\tilde{\sigma}_{NC}$ and $\tilde{\sigma}_{CC}$. In Fig. 6 this comparison is shown. Without a detailed analysis one observes that the u-valence quark distribution is about 1.5 to 3 times larger than the d quark distribution at $x = 0.3$ and $Q^2 \geq 2000$ GeV^2.

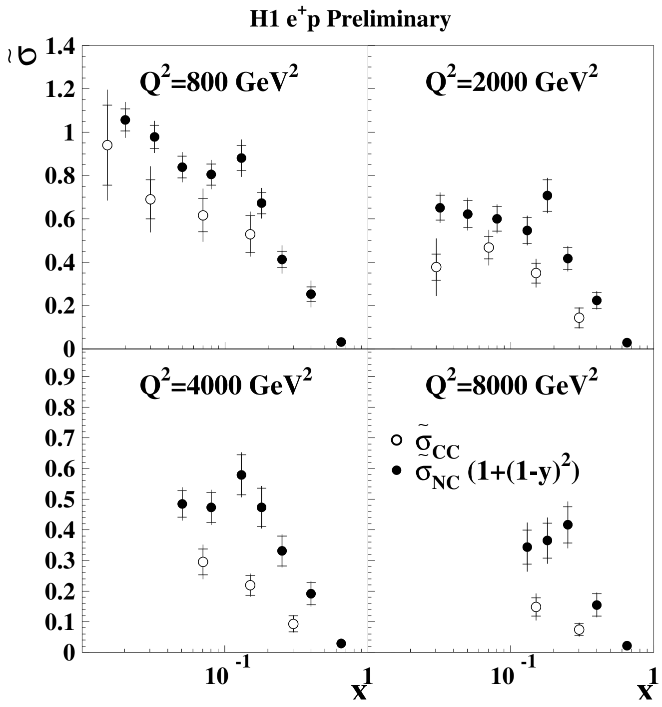

Figure 6: Comparison of reduced double differential cross sections of NC and CC as function of x in bins of Q^2.

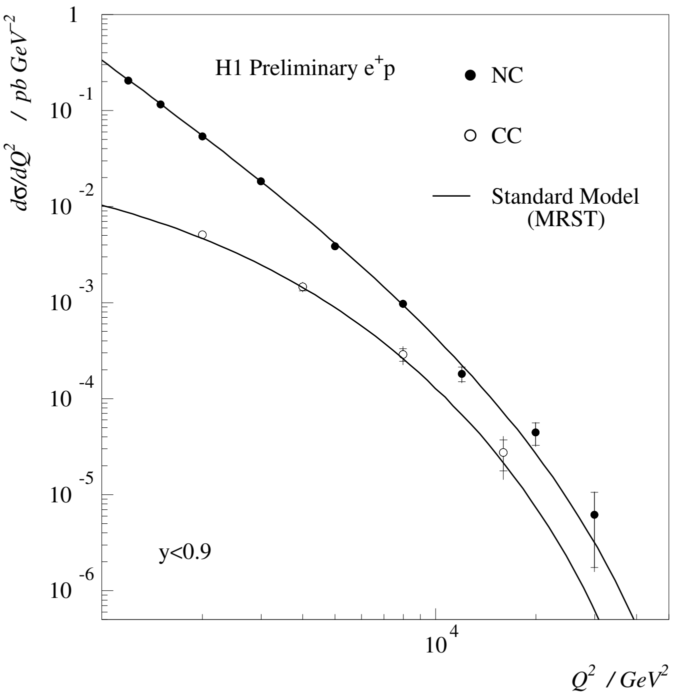

Figure 7: The NC and CC single differential cross section $d\sigma/dQ^2$ compared with the Standard Model predictions.

3.8 *Test of the W Propagator Term*

The Q^2 dependence of the CC cross section (see Fig. 7), which is governed by the propagator term $M_W^2/(Q^2+M_W^2)$, is used for a measurement of the W-mass in the space like regime. By using $G_F = 1.16639 \times 10^{-5}$ GeV^2 according to [22] and by fitting the shape of the CC double differential cross section a mass

$$M_W = 81.2 \pm 3.3(stat.) \pm 4.3(syst.) \text{ GeV}$$

has been determined. Here the main systematic error is due to the $3-4\%$ uncertainty of the hadronic energy scale of the LAr calorimeter. An additional 2.8 GeV uncertainty is due to effects of different parton density functions and radiative corrections.

The H1 result for M_W is in good agreement with direct and indirect measurements performed in other channels [23]. No evidence for any unexpected structure in the space like electroweak propagator is visible.

4 Summary

Neutral and charged current interactions at high Q^2 have been investigated in e^+p collisions using the H1 detector at HERA.

Single and double differential neutral current cross sections have been measured, which are found to be in good agreement to the Standard Model predictions. In the region of $Q^2 > 15000$ GeV^2 a slight excess is visible, but with less significance compared to previously published results. In the kinematic domain of very high Q^2 the sensitivity in NC DIS to the exchange of the Z boson was investigated. For a $Q^2 > 10000$ GeV^2 good agreement was found to the predictions of the Standard Model, taking into account the effects due to the γZ interference.

In the high Q^2 charged current sector the double differential cross section has been measured for the first time at HERA. Also the CC cross section is found to be in good agreement with the Standard Model predictions, though the accuracy is still statistically limited. A fit to the Q^2 dependence of the CC cross section yielded a value of the propagator mass $M_W = 81.2 \pm 5.4$ GeV^2 in space like lepton nucleon scattering.

A comparison of NC and CC cross sections at high x illustrates the feasibility of testing the u/d ratio in the valence quark region.

Acknowledgements

I am grateful to my colleagues in the H1-"ELAN" and "EW" physics working groups, whose outstanding efforts made these results possible. Warm thanks to B. Heinemann for all technical help in preparing the contribution.

I like to use this opportunity to thank D. Wegener for his pleasant and continuous support and all fruitful discussions. It has been a pleasure to work in the frame of Dortmund University E5 group under his leadership.

This work was supported by the Bundesministerium für Bildung, Wissenschaft, Forschung und Technologie, FRG, under the contract number 57DO55P.

References

1. H1 Collaboration, S. Aid et al., Nucl. Phys. **B470** (1996) 3.
2. M. Klein, H1 Collaboration, these proceedings.
3. H1 Collaboration, "Measurement of Neutral and Charged Current Cross-Sections at High Q^2", Paper 533, submitted to this conference.
4. A.Blondel, F.Jacquet, Proceedings of the Study of an *ep* Facility for Europe, ed. U.Amaldi, DESY 79/48 (1979) 391.
5. U. Bassler and G. Bernardi, DESY 97-137 (1997), submitted to Nucl. Instr. Meth.
6. H1 Collaboration, I. Abt et. al., Nucl. Instr. Meth. **A386** (1997) 310 and 348.
7. H1 Calorimeter Group, B. Andrieu et al., Nucl. Instr. Meth. **A336** (1993) 460.
8. M. Fleischer, "Performance of the H1 Liquid Argon Calorimeter", DESY 98-005 (1998), to appear in: Proceedings of CALOR97.
9. H1 Collaboration, T. Ahmed et al., Z. Phys. C66 (1995) 529.
10. H1 Collaboration, "Luminosity Measurement in the H1 Experiment at HERA", ICHEP 96-Warsowie, pa17-026.
11. R. Brun et al., GEANT3 User's Guide, CERN-DD/EE-84-1 (1987).
12. G. A. Schuler and H. Spiesberger, Proceedings of the Workshop Physics at HERA, vol. 3, eds. W. Buchmüller, G. Ingelman, DESY (1992) 1419.
13. A. Kwiatkowski, H. Spiesberger and H.-J. Möhring, Comp.Phys.Comm. **69** (1992) 155.
14. L. Lönnblad, Comp.Phys.Comm. **71** (1992) 15.
15. G. Ingelman, Proceedings of the Workshop Physics at HERA, vol. 3, eds. W. Buchmüller, G. Ingelman, DESY (1992) 1366.
16. A.D Martin, W.J. Stirling and R.G. Roberts, Phys. Lett. **B306** (1993) 145; **B309** (1993).
17. A. Arbuzov et. al., DESY 95-185 (1995).
18. Y. L. Dokshitzer, Sov. Phys. JETP **46** (1977) 641; V. N. Gribov and L.N. Lipatov, Sov. J. Nucl. Phys. **15** (1972) 438 and 675;
    G. Altarelli and G. Parisi, Nucl. Phys. **B126** (1977) 297.
19. H1 Collaboration, C. Adloff et al., Z. Phys **C74** (1997) 191.
    ZEUS Collaboration, J. Breitweg et al., Z. Phys. **C74** (1997) 207.
20. A. Martin et al., RAL-TR-98-029.
21. H1 Collaboration, "A Measurement of the Inclusive Deep Inelastic *ep* Scattering Cross Section at low Q^2 at HERA", IECHEP 97-Jerusalem, 97-260 (1997).
22. C. Caso et al, Eur. Phys. J. **C3** (1998) 1.
23. CDF Collaboration, F. Abe et al., Phys. Rev. Lett. 75, (1995) 11; Phys.Rev. **D 52** (1995) 4784.
    DØ Collaboration, B. Abbott et al., FERMILAB PUB-97/422-E (1997), submitted to Phys.Rev.
    ALEPH Collaboration, R. Barate et al., Phys. Lett. **B422** (1998) 384.
    DELPHI Collaboration, P. Abreu et al., Eur.Phys.J. **C2** (1998) 581.
    L3 Collaboration, M. Acciarri et al., Phys. Lett. **B413** (1997) 176.
    OPAL Collaboration, K. Ackerstaff et al., Eur.Phys.J. **C1** (1998) 395.